

Balanced liquid metal reconfigurable microstrip filter

Arcesio Arbelaez-Nieto, Jose-Luis Olvera-Cervantes, Carlos E. Saavedra & Alonso Corona-Chavez

To cite this article: Arcesio Arbelaez-Nieto, Jose-Luis Olvera-Cervantes, Carlos E. Saavedra & Alonso Corona-Chavez (2017): Balanced liquid metal reconfigurable microstrip filter, Journal of Electromagnetic Waves and Applications, DOI: [10.1080/09205071.2017.1351402](https://doi.org/10.1080/09205071.2017.1351402)

To link to this article: <http://dx.doi.org/10.1080/09205071.2017.1351402>



Published online: 12 Jul 2017.



Submit your article to this journal [↗](#)



Article views: 14



View related articles [↗](#)



View Crossmark data [↗](#)



Balanced liquid metal reconfigurable microstrip filter

Arcesio Arbelaez-Nieto^a, Jose-Luis Olvera-Cervantes^a, Carlos E. Saavedra^c and Alonso Corona-Chavez^{a,b}

^aNational Institute of Astrophysics, Optics and Electronics, Puebla, Mexico; ^bDepartamento de Electronica, DICIS, Universidad de Guanajuato, Campus Irapuato-Salamanca, Salamanca, Mexico; ^cDepartment of Electronics, Queen's University, Kingston, Canada

ABSTRACT

A reconfigurable balanced resonator and a reconfigurable Balanced Band-Pass Filter (BBPF) are presented in this work. The resonator is based on closed-loop transmission lines, two parallel lines and two T-sections. Reconfigurability is achieved using Eutectic Galium–Indium (EGaIn) liquid metal. A third-order reconfigurable filter was designed, fabricated, and measured to work at 2 and 1.65 GHz.

ARTICLE HISTORY

Received 3 February 2017
Accepted 12 April 2017

KEYWORDS

Bandpass filter; reconfigurable; differential signaling; resonator; liquid metal

1. Introduction

The evolution of the telecommunications is producing the rise of new challenges in devices and technology. Balanced structures with differential signaling are good options to deal with two of these challenges, noise and EMI (Electromagnetic Interference) [1–3]. A reconfigurable filter is a device with the capability to filter signals at two or more frequency bands using any kind of system to modify its electrical configuration. Also, these reconfigurable filters are required to support new multi-band systems as 5G mobile technology or multi-standard front-ends [4]. Two types of reconfigurable filters are available; first type has a discrete number of states and second class has a continuous adjustment range, usually called tunable filters. Some alternatives to build these filters are: integrated filters [5], MEMS's-based filters [6], SAW filters [7], and liquid metal-based filters [8]. However, a limited amount of balanced reconfigurable filters can be found in the literature and these are built using conventional variable lumped devices such as varactors or diodes [9,10].

The problems with these lumped devices include additional insertion losses, limited power handling, and non-linearities, which require a design process more complicated and a bias network carefully designed.

On the other hand, liquid metal-based reconfigurable filters can support high power in comparison with conventional methods [11], these have no linearity problems and a bias network is not required to supply energy directly to the filter. However, fluidic channels are necessary, sometimes in micro-metric scale, which are an engineering challenge considering that it is not a field directly related with electronics [12–14].

Two main problems to solve in reconfigurable filters are the variability of the quality factors and the mutual coupling factors. If a stable bandwidth is required, the quality factor should be the same for both states; however, if the electrical configuration of the resonator is modified, the quality factor will be different for every state [2]. In differential resonators, the current concentration is higher in the virtual ground, for this reason the high current ends of each resonator cannot be too close or too far to adjust the required mutual coupling factor, which is harder for non-conventional resonators with more complex structures. The input/output ports are used to adjust the external quality factor but the mutual coupling factor should be adjusted without additional complexity using the same mechanism.

This paper reports the design and experimental verification of a balanced reconfigurable microstrip filter. The reconfigurability is based on liquid metal droplets generating a short circuit which produces two different states under differential-mode operation and two states under common-mode operation.

2. Balanced liquid metal reconfigurable resonator

The proposed resonator is composed by two closed-loop transmission lines, two parallel lines with electrical length θ_p and impedance Z_p and two T-sections as shown in Figure 1. The T-sections are connected/disconnected by the presence/absence of the liquid metal at the point A. Close-loop transmission lines are the main resonant structure, while the parallel

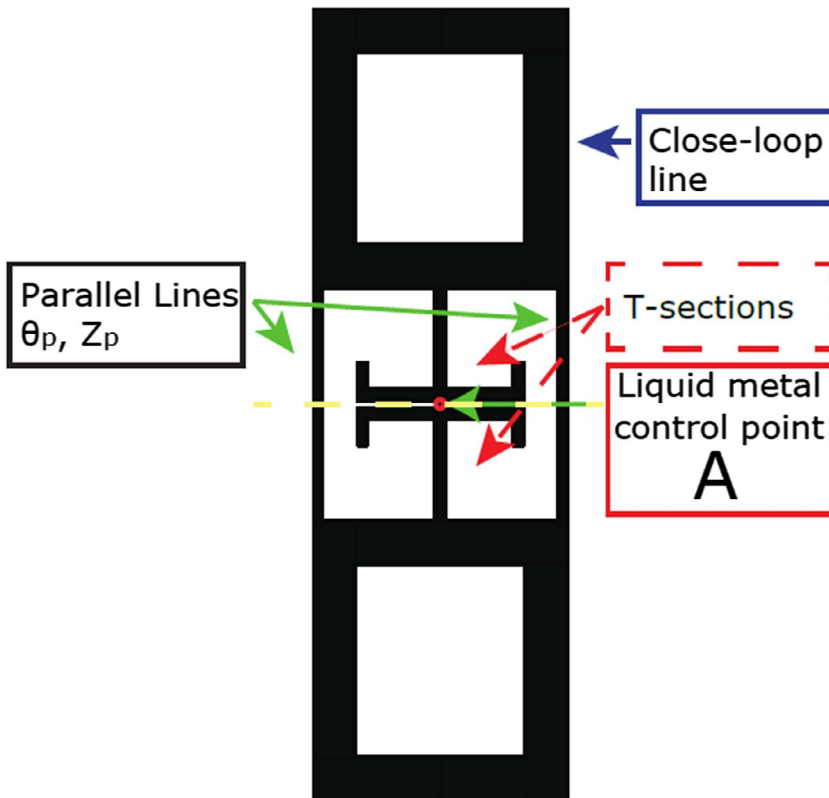


Figure 1. Proposed resonator.

transmission lines are used to adjust the input/output quality factors and the mutual coupling factors between resonators. Additionally, a central line is used to get the reconfigurability of the resonator with minimal alteration of the quality and mutual coupling factors due to the high current concentration around the virtual ground.

There is a virtual short circuit (electric wall) under differential-mode operation along the symmetry line due to the symmetry of the circuit [15]. On the other hand, under common-mode operation a virtual open circuit (magnetic wall) is generated along the symmetry line. Then, it is possible to obtain two states under differential-mode operation and two states under common-mode operation.

2.1. Equivalent circuit and operation of the first state

First state is obtained considering differential-mode operation. Here, the T-sections are connected generating the first band centered at f_1 . In this state, the T-sections are simplified by a single transmission line (with electrical length θ_3 and Z_3) due to short circuit at point A as is shown in Figure 2(a).

The resonant frequency is found, where the denominator of the input impedance is equal to zero [16]. The input impedance is calculated from even/odd-mode analysis. In this paper, only the even-mode equivalent will be analyzed because the resonant frequency (related to Z_{evend}) of this mode is lower than the resonant frequency of the odd-mode in the same manner as is shown in [17]. The odd-mode and even-mode equivalent circuits for the differential-mode operation are shown in Figure 3.

The even-mode input impedance Z_{evend} can be calculated using the Equation (1).

$$Z_{\text{evend}} = \frac{1 + Z_{\text{in}} Y_{22a}}{Z_{\text{in}} (Y_{11a} Y_{22a} - Y_{12a} Y_{21a}) + Y_{22a}}, \quad (1)$$

where

$$Y_{11a} = Y_{22a} = \frac{-j \cot(\theta_1)}{Z_1}, \quad (2)$$

$$Y_{12a} = Y_{21a} = \frac{j \csc(\theta_1)}{Z_1}, \quad (3)$$

$$Z_{\text{in}} = \frac{Z_{\text{in1}} Z_{\text{in2}}}{(Z_{\text{in1}} + Z_{\text{in2}})}, \quad (4)$$

$$Z_{\text{in1}} = \frac{1 + Z Y_{22b}}{Z (Y_{11b} Y_{22b} - Y_{12b} Y_{21b}) + Y_{22b}}, \quad (5)$$

$$Y_{11b} = Y_{22b} = \frac{-j \cot(\theta_2)}{Z_2}, \quad (6)$$

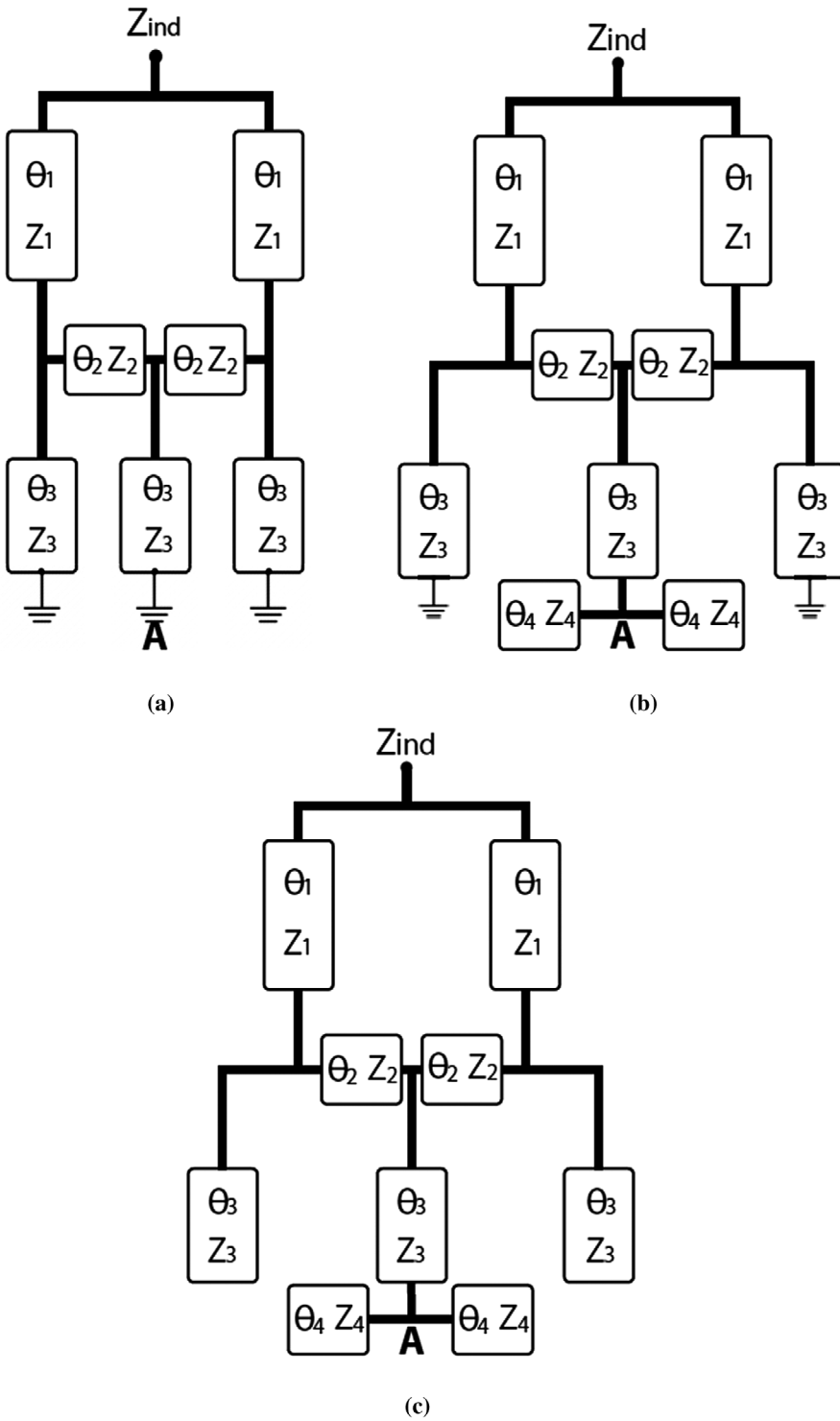


Figure 2. Equivalent circuits of the resonator under differential and common mode for both states. (a) First state under differential-mode operation. (b) Second state under differential-mode operation. (c) First and second states under common-mode operation.

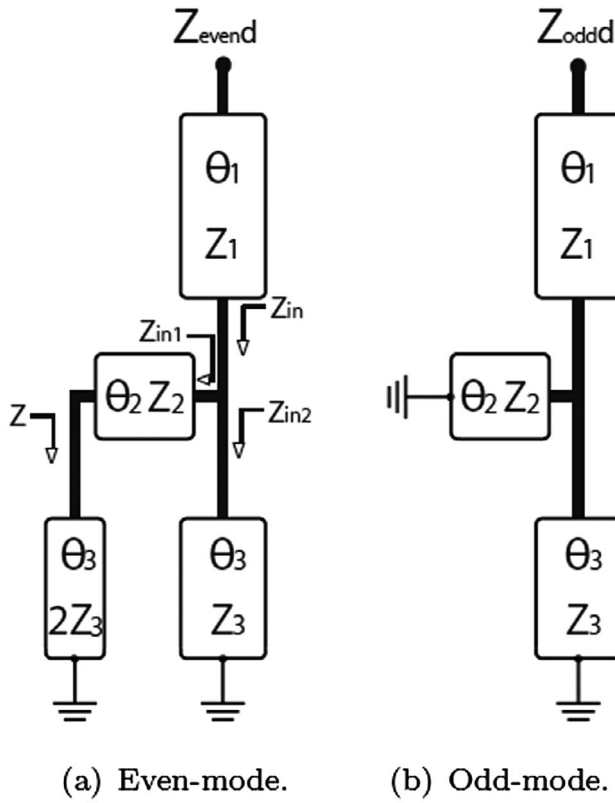


Figure 3. Equivalent circuits for even–odd analysis. (a) Even-mode. (b) Odd-mode.

$$Y_{12b} = Y_{21b} = \frac{j\csc(\theta_2)}{Z_2}, \tag{7}$$

$$Z = 2jZ_3 \tan\theta_3, \tag{8}$$

$$Z_{in2} = jZ_3 \tan\theta_3, \tag{9}$$

Some additional conditions to simplify solving the Equation (1) are: $Z_2 = Z_1$, $\theta_2 = \theta_1/3$, $Z_3 = 2Z_1$. A mathematics software tool or an analytic method can be used to solve the denominator of the even-mode input impedance Z_{evenD} , and an additional software tool can be used to synthesize the transmission lines of the required electrical length and characteristic impedance at the desired resonance frequency.

2.2. Equivalent circuit and operation of the second state

The second state is obtained by considering differential-mode operation and “floating contact-point”. This generates a second band centered at f_2 . The equivalent circuit is given by the circuit in Figure 2(b). In this case, there are two ways to define the operation frequency of the second state. First, using the analytic expression for the even-mode input impedance

in Figure 2(b). The second alternative is to use a simulation approach based on circuital or full-wave simulations, where a sweep of the parameter θ_4 is done once all the physical dimensions of the first state have been defined.

Considering that the influence of the impedance on the resonance frequency is low when the ratio Z_4/Z_3 is around 1 [18], this ratio can be used to miniaturize the resonator length; therefore, the easiest way to define the characteristic impedance of the arms is to choose the same impedance of the stubs Z_3 .

The initial frequency separation between resonant frequencies of both states can be defined as $f_1 - f_2$, where f_1 is the resonant frequency of the first state and f_2 is the resonant frequency of the second state. Then, the resonant frequency of the second state can be adjusted only below the frequency of the first state f_1 which has been defined previously.

The resonant frequency of the second state can be obtained replacing the input impedance Z in Equation (8) by the input impedance of a transmission line with an open circuit termination loaded with another opened transmission line.

2.3. Equivalent circuit and operation of the first state under common-mode operation

This state is obtained considering common-mode operation and connected T-sections. In this state, T-sections and parallel lines are opened as is shown in Figure 2(c). An important characteristic of the reconfigurable resonator is the impossibility to get a second state under common-mode operation because there is an open circuit at the end of the central stub even in presence of liquid metal. The resonator's equivalent circuit for even-mode under common-mode operation is shown in Figure 4.

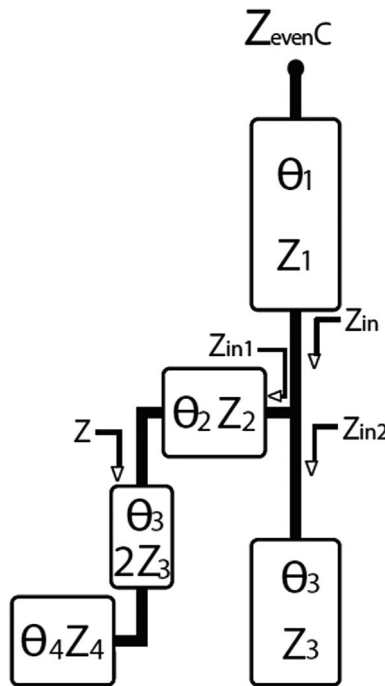


Figure 4. Even-mode equivalent circuit under common-mode operation for both states.

The input impedance of the even-mode under common-mode operation can be calculated using Equation (10).

$$Z_{evenc} = \frac{1 + Z_{in} + Y_{22a}}{Z_{in}(Y_{11a}Y_{22a} - Y_{12a}Y_{21a}) + Y_{22a}}, \quad (10)$$

where

$$Y_{11a} = Y_{22a} = \frac{-j\cot(\theta_1)}{Z_1}, \quad (11)$$

$$Y_{12a} = Y_{21a} = \frac{j\csc(\theta_1)}{Z_1}, \quad (12)$$

$$Z_{in} = \frac{Z_{in1}Z_{in2}}{(Z_{in1} + Z_{in2})}, \quad (13)$$

$$Z_{in1} = \frac{1 + ZY_{22b}}{Z(Y_{11b}Y_{22b} - Y_{12b}Y_{21b}) + Y_{22b}}, \quad (14)$$

$$Y_{11b} = Y_{22b} = \frac{-j\cot(\theta_2)}{Z_2}, \quad (15)$$

$$Y_{12b} = Y_{21b} = \frac{j\csc(\theta_2)}{Z_2}, \quad (16)$$

$$Z = \frac{1 + Z_x Y_{22c}}{Z_x (Y_{11c} Y_{22c} - Y_{12c} Y_{21c})}, \quad (17)$$

$$Z_x = jZ_4 \cot\theta_4, \quad (18)$$

$$Y_{11c} = Y_{22c} = \frac{-j\cot(\theta_3)}{2Z_3}, \quad (19)$$

$$Y_{12c} = Y_{21c} = \frac{j\csc(\theta_3)}{2Z_3}, \quad (20)$$

$$Z_{in2} = jZ_3 \cot(\theta_3), \quad (21)$$

2.4. Equivalent circuit and operation of the second state under common-mode operation

The last case is obtained considering common-mode operation when the T-sections are disconnected. Here, the parallel lines are opened which leads to the same equivalent circuit as in the previous section (Figure 4).

2.5. Design procedure of the resonator

The resonator's design procedure can be summarized as follows:

- (1) *Selection of the operating frequency for the first state.* Frequency of the first state (f_1) is chosen, then, all the electrical lengths of the transmission lines can be found by solving the numerator of Equation (1).
- (2) *Selection of the materials.* Appropriate microwave substrate is chosen to define the physical dimensions of the required transmission lines.
- (3) *Selection of the operating frequency for the second state.* Frequency of the second state (f_2) is chosen to be lower than f_1 , the lower limit to choose f_1 is defined by the maximum physical length of the T-section's arms that can be put within the available space between the parallel lines and the T-sections. It means that is not possible to use a large arm to get a lower frequency because it is not possible to accommodate the arm (transmission line) even if it is bent.
- (4) *Tuning of the resonator.* A full-wave simulation is used to tune the response of both states.

3. Balanced third order reconfigurable filter

A prototype filter was fabricated to show the viability of the resonator to build reconfigurable filters.

3.1. Resonator's design

To illustrate the design procedure of the resonator, a basic resonator cell was designed using the design procedure described above.

- First step (f_1):

The first state is designed to work at 2 GHz. Firstly, some parameters are chosen depending on the physical constrains or convenience: $\theta_1 = 57^\circ$, $Z_1 = Z_2 = 50 \Omega$, $Z_3 = 2Z_2 = 100 \Omega$, and $\theta_2 = \theta_1/3 = 19^\circ$. The electrical length of the stubs can be calculated by solving the denominator of the Equation (1). There are two possible solutions but the negative solution is discarded because it has no physical meaning. The electrical length of transmission line is $\theta_3 = 21.1^\circ$.

- Second step (materials):

The resonator was built using the substrate Rogers RO4003C ($\epsilon_r = 3.55$, $h = 0.81$ mm, and loss tangent = 0.0022), the liquid metal chosen to build the prototype was Eutetic Galium–Indium (EGaln) with a conductivity of 3.46×10^6 S/m.

- Third step (f_2):

The second state is designed to work at $f_2 = 1.65$ GHz. The required electrical length θ_4 can be obtained from Figure 5. If the desired frequency f_2 is 1.6 GHz then the electrical length of the line θ_4 should be around 19.08° which corresponds to 5 mm. As can be seen, the frequency decrease when the length is increased, this effect can be associated to the increasing of the electrical length and the guided wavelength.

- Fourth step:

After full-wave optimization, the final physical dimensions of the transmission lines are shown in Table 1. The current distribution plot in Figure 6 shows the high-current concentration around virtual ground on the parallel lines which guarantees a high-external quality factor and a good mutual coupling factor between adjacent resonators.

3.2. Filter's design

To demonstrate the concept, a differential reconfigurable filter was designed and fabricated using the following design parameters: Butterworth response, central frequency of the first state $f_1 = 2$ GHz, fractional bandwidth of both states $FBW = 10\%$, central frequency of the second state between 300 and 600 MHz lower than the frequency of the first state (1500–1900 MHz), in this case $f_2 = 1.65$ GHz.

Design parameters of the filter are: $N = 3$, $FBW = 10\%$, $g_0 = 1$, $g_1 = 1$, $g_2 = 2$, $g_3 = 1$, and $g_4 = 1$, external input/output quality factor $Q_e = 10$, mutual coupling factor $M_{12} = M_2 = 0.071$.

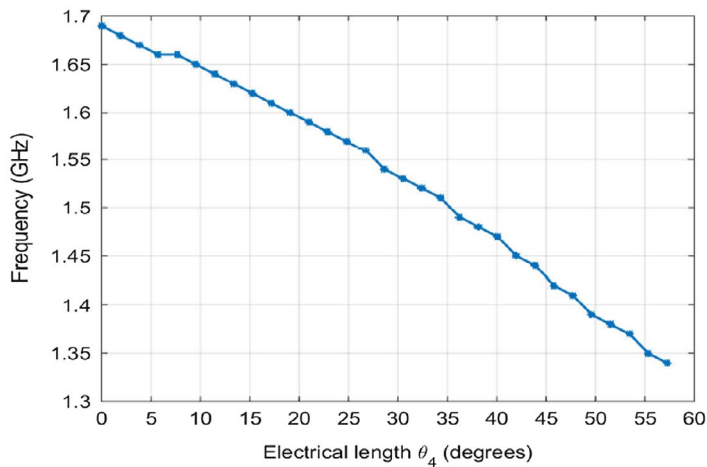


Figure 5. Variation of the resonance frequency of the second state with the parameter θ_4 .

Table 1. Physical dimensions of the resonator.

Line	Length (mm)	Width (mm)
θ_1	14.25	1.8
θ_2	4.75	1.8
θ_3	5.5	0.45
θ_4	4.4	0.45

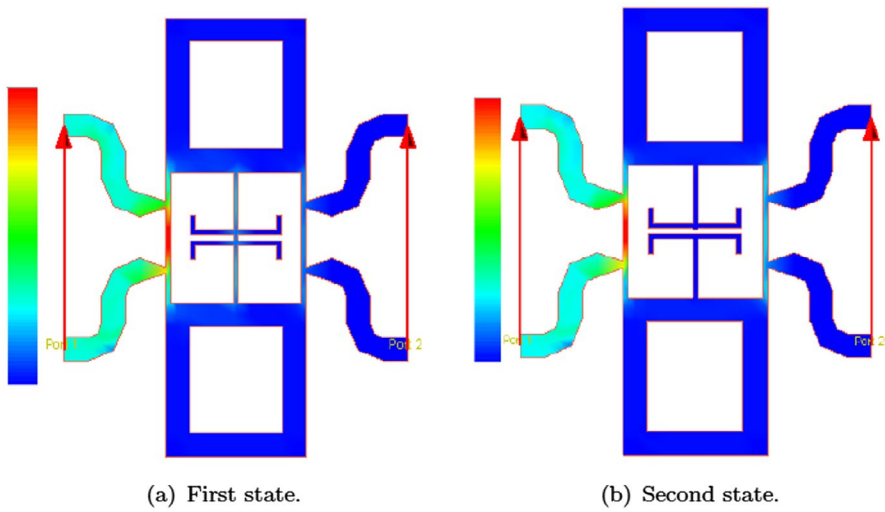


Figure 6. Resonator's current distribution at 2 GHz. (a) First state. (b) Second state.

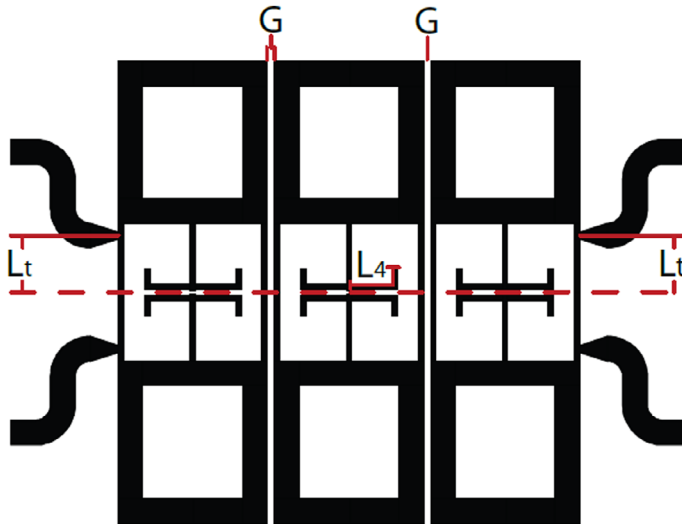


Figure 7. Layout of the fabricated Filter $G = 0.5$ mm, $L_t = 4.1$ mm, and $L_4 = 4.4$ mm.

A small separation gap of 0.3 mm between the central stubs was used to deposit the droplet of liquid metal and it is contained by a small transparent plastic cylinder with a radius of 0.5 mm. The amount of liquid metal is less than 0.5 ml per droplet. The prototype filter is manually reconfigured but there are some alternatives to control the liquid metal as can be seen in Refs. [12,13]. There, the droplet position is controlled using a liquid carrier which responds to electric fields or also can be used a pump to change the location of the liquid metal, respectively. The final dimensions of the filter are shown in Figure 7 and a picture of the fabricated filter is shown in Figure 8.

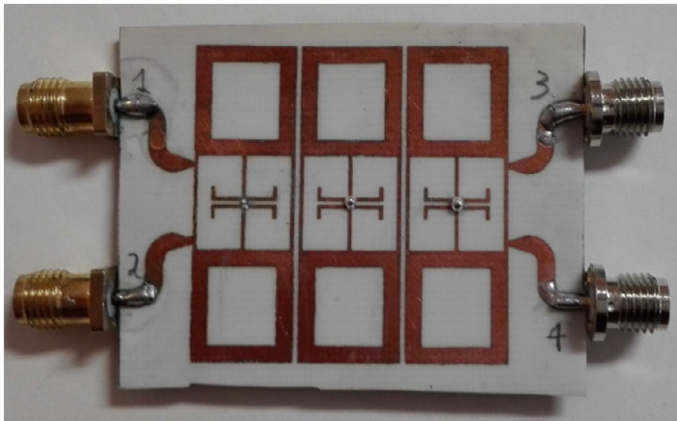


Figure 8. Fabricated prototype filter.

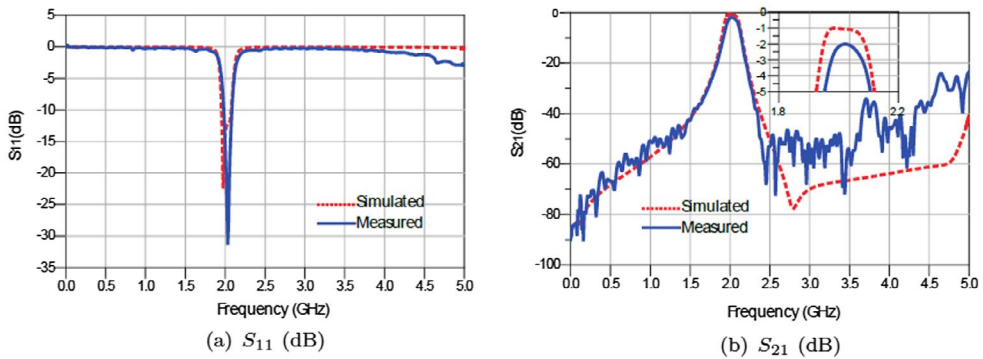


Figure 9. Simulated and measured differential-mode S-parameters of the first state at 2 GHz. (a) S_{11} (dB). (b) S_{21} (dB).

4. Experimental results

Two sets of four port S-parameters were measured using a two port VNA (Teledyne LeCroy SPARQ 3002E) then the differential-mode and common-mode S-parameters were obtained by transformation of the four port single-ended S-parameters as is described in [2].

4.1. Differential-mode operation

Figure 9 shows the S-parameters of the first state. The central frequency of the fabricated filter is 2.029 GHz, the bandwidth is 7.5%, the return loss is better than 10 dB and the insertion loss is 2 dB. The Attenuation at 1.65 GHz is 35 dB. In this case the insertion loss is increased and the bandwidth is decreased due to the lower EGaln’s conductivity around 17 times less than the cooper’s conductivity.

Figure 10 shows the S-parameters of the second state of the reconfigurable filter. The central frequency is 1.64 GHz, the bandwidth is 10.9%, return loss is better than 10 dB and the insertion loss is 1.598 dB. Additionally, the attenuation at 2 GHz is 37 dB.

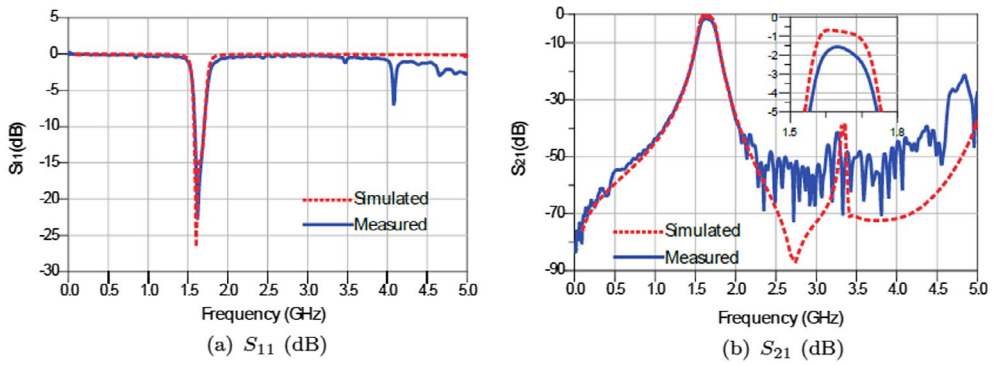


Figure 10. Simulated and measured differential-mode S-parameters of the second state at 1.65 GHz. (a) S_{11} (dB). (b) S_{21} (dB).

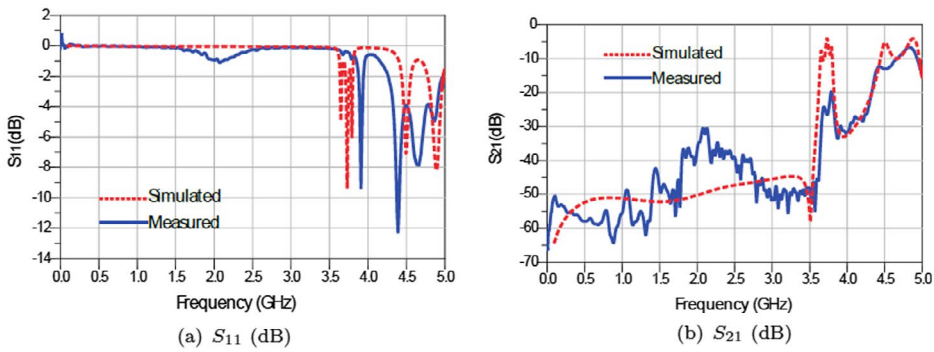


Figure 11. Simulated and measured differential-mode S-parameters of both states under common-mode operation. (a) S_{11} (dB). (b) S_{21} (dB).

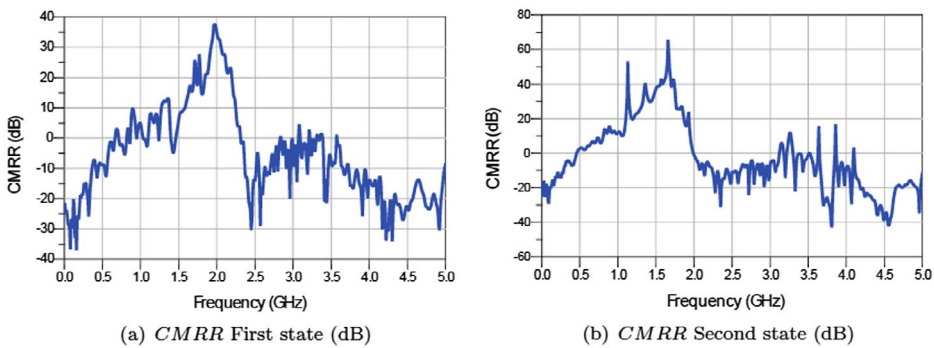


Figure 12. Measured CMRR for both states. (a) CMRR first state (dB). (b) CMRR second state (dB).

4.2. Common-mode operation

Figure 11 shows the S-parameters under common-mode operation. The filter exhibits good common-mode attenuation better than 30 dB around the operation band and the worst case attenuation is 6.7 dB at 4.83 GHz.

The filter's CMRR is calculated from its measured S-parameters using the Equation $20\log|S_{21}^{DM}/S_{21}^{CM}|$, where DM stands for differential-mode and CM for common-mode. A CMRR vs. frequency plot is shown in Figure 12 and it shows that its peak value is 37.6 dB at 1.97 GHz and better than 30 dB at the passband of the first state and 65.7 dB at 1.66 GHz, and better than 40 dB at the passband of the second state.

5. Conclusions

A balanced reconfigurable resonator and a reconfigurable BBPF based on close-loop resonator with parallel lines, T-sections and liquid metal were proposed, designed, and measured. The measured results are in a good level of agreement with simulated results. The common-mode rejection is better than 30 dB at the first band and it is better than 40 dB at the second band. The worst case of the insertion loss is around 2 dB when liquid metal is used to generate the short circuit which shows the viability to use EGaln in this kind of reconfigurable resonators.

Disclosure statement

No potential conflict of interest was reported by the authors.

Funding

This work was supported by Prodep-NPTC [grant number 185003].

References

- [1] Shiue GH, Shiu JH, Chiu PW. Analysis and design of crosstalk noise reduction for coupled striplines inserted guard trace with an open-stub on time-domain in high-speed digital circuits. *IEEE Transactions on Components, Packaging and Manufacturing Technology*. 2011;1(10):1573–1582.
- [2] Arbelaez-Nieto A, Cruz-Perez E, Olvera-Cervantes JL, et al. The perfect balance-a design procedure for balanced bandpass filters [application notes]. *IEEE Microwave Mag*. 2015;16(10):54–65.
- [3] Kaur M, Kakar S, Mandal D. Electromagnetic interference. *IEEE 3rd International Conference on Electronics Computer Technology (ICECT)*. Vol. 4; 2011. p. 1–5.
- [4] Vidojkovic M. Configurable circuits and their impact on multi-standard rf front-end architectures. *Netherlands: Technische Universiteit Eindhoven*; 2011.
- [5] Lu R, Lu Z, Chen D, et al. A 4th-order n-path filter in 40 nm cmos with tunable gm-c stage and reduced center-frequency offset. *IEEE 11th International Conference on ASIC (ASICON)*; 2015 Nov. p. 1–4.
- [6] Alazemi AJ, Rebeiz GM. A low-loss 1.4 ghz-2.1 ghz compact tunable three-pole filter with improved stopband rejection using rf-mems capacitors. *IEEE MTT-S International Microwave Symposium (IMS)*; 2016 May. p. 1:4.
- [7] Wada T, Ogami T, Horita A, et al. A new tunable saw filter circuit for reconfigurable rf. *IEEE MTT-S International Microwave Symposium (IMS)*; 2016 May. p. 1–4.
- [8] Khan MR, Hayes GJ, Zhang S, et al. A pressure responsive fluidic microstrip open stub resonator using a liquid metal alloy. *IEEE Microwave Wireless Compon Lett*. 2012 Nov;22(11):577–579.

- [9] Li YC, Xue Q. Tunable balanced bandpass filter with constant bandwidth and high common-mode suppression. *IEEE Trans Microwave Theory Tech.* **2011 Oct**;59(10):2452–2460.
- [10] Deng PH, Jheng JH. A switched reconfigurable high-isolation dual-band bandpass filter. *IEEE Microwave Wireless Compon Lett.* **2011 Feb**;21(2):71–73.
- [11] Saghati AP, Batra JS, Kameoka J, et al. A miniaturized micro fluidically reconfigurable coplanar waveguide bandpass filter with maximum power handling of 10 watts. *IEEE Transactions Microwave Theory Tech.* **2015 Aug**;63(8):2515–2525.
- [12] Koo C, LeBlanc BE, Kelley M, et al. Manipulating liquid metal droplets in microfluidic channels with minimized skin residues toward tunable RF applications. *J Microelectromech Syst.* **2015 Aug**;24(4):1069–1076.
- [13] Palomo T, Mumcu G. Microfluidically reconfigurable metallized plate loaded frequency-agile RF bandpass filters. *IEEE Trans Microwave Theory Tech.* **2016 Jan**;64(1):158–165.
- [14] Saghati AP, Batra J, Kameoka J, et al. Microfluidically-tuned miniaturized planar microwave resonators. *Wireless and Microwave Technology Conference (WAMICON), IEEE 15th Annual*; **2014**. p. 1–3.
- [15] Pelaez JE, Olvera-Cervantes JL, Corona-Chavez A. Novel common mode suppression network for the transformation of single-ended to balanced filters. *Microwave Opt Technol Lett.* **2016**;58(12):2831–2833.
- [16] Olvera-Cervantes JL, Corona-Chavez A. Microstrip balanced bandpass filter with compact size, extended-stopband and common-mode noise suppression. *IEEE Microwave Wireless Compon Lett.* **2013**;23(10):530–532.
- [17] Sun SJ, Lin L, Wu B, et al. A novel quad-mode resonator and its application to dual-band bandpass filters. *Prog Electromagnet Res Lett.* **2013**;43:95–104.
- [18] Sagawa M, Makimoto M, Yamashita S. Geometrical structures and fundamental characteristics of microwave stepped-impedance resonators. *IEEE Trans Microwave Theory Tech.* **1997 Jul**;45(7):1078–1085.